IEEE Access
Multidisciplinary ⋮ Rapid Review ⋮ Open Access Journal

Digital Object Identifier 10.1109/ACCESS.2025.00125

Extended State Observer Based Robust Model Predictive Velocity Control for Permanent Magnet Synchronous Motor

Eunji Lee[1], Yonghao Gui[2] (Senior Member, IEEE), Sesun You[3], Jun Moon[4] (Senior Member, IEEE), and Wonhee Kim[5] (Member, IEEE)

[1]Department of Energy Systems Engineering, Chung-Ang University, Seoul, South Korea
[2]Electrification and Energy Infrastructures Division, Oak Ridge National Laboratory, Knoxville, United States
[3]Department of Electrical Engineering, Keimyung University, Daegu, South Korea
[4]Department of Electrical Engineering, Hanyang University, Seoul, South Korea
[5]School of Energy Systems Engineering, Chung-Ang University, Seoul, South Korea

Corresponding author: Sesun You (e-mail: yousesun@kmu.ac.kr), Jun Moon (e-mail: junmoon@hanyang.ac.kr), and Wonhee Kim (e-mail: whkim79@cau.ac.kr)

ABSTRACT This article proposes an extended state observer based robust model predictive velocity control to decrease system prediction error under parameter uncertainties for permanent magnet synchronous motor (PMSM). We develop a new PMSM model that consists of velocity and acceleration to lump the system information and an external disturbance into a disturbance. The extended state observer (ESO) is designed to estimate the velocity, acceleration, and disturbance. By estimating the state variables and disturbance using the ESO, the model predictive control (MPC) finds the optimal control input by predicting future system behavior. Additionally, the direct current controller is designed so that the direct current converges to zero. Because the proposed method is not designed based on the cascade structure from the viewpoint of velocity control, the optimization control for the velocity and currents can be defined. Thus, the proposed method is robust against external disturbances and parameter uncertainties owing to feedback linearization, state feedback, and ESO-based MPC using the acceleration PMSM model. The proposed control algorithm was experimentally verified and it showed improved velocity tracking performance compared with ESO-based MPC using the conventional PMSM model.

INDEX TERMS Model predictive control, Extended state observer, Feedback linearization, Permanent magnet synchronous motor, Velocity tracking.

I. INTRODUCTION

PERMANENT magnet synchronous motor (PMSM) have been widely used in various applications, such as industrial robots, electric vehicles, and air conditioners because of their high efficiency, low maintenance cost, and high torque-to-current ratio [1]-[2]. However, it is difficult to guarantee high control performance for a PMSM because it is a nonlinear system with two inputs and its control performance is affected by the existence of nonlinearities, parameter uncertainties, unmodeled dynamics, and load torque [3]. To address these problems, various control methods have been developed for PMSM systems over the past few decades. Proportional-integral-derivative (PID) control has been widely used in various applications because of its effectiveness and simplicity of design without considering the system's model. Nevertheless, a significant limitation of the conventional PID controller is its sensitivity to system uncertainties, which degrades control performance [4]-[5]. To solve these problems, various control methods have been proposed and applied to PMSM systems, such as sliding mode control [6], adaptive control [7]-[8], fuzzy control [9], disturbance observer based control [10]-[11], and model predictive control (MPC) [12]. Among the aforementioned advanced control methods, optimization control methods have been more thoroughly studied in recent years to achieve high control performance.

Model predictive control, as an optimal control method, has received increasing attention owing to its online optimization ability, simple structure, and easy-to-include constraints [13]-[14]. However, for several decades, MPC was only successfully applied in the process and chemical industries because of its complicated models and slow rate dynamics [15]. With the rapid increase in computing hardware performance in recent years, MPC has been widely implemented in many applications, such as machine drives [16], controllable power

supplies [17], and grid-connected inverters [18]. In general, the MPC algorithm is based on the repeated real-time optimization of a mathematical system model, particularly regarding in the PMSM model [19]. For every sampling time, MPC calculates the future control action sequence by minimizing a cost function to include a control objective and uses only the first element of this control action sequence [20]. Thus, the MPC method predicts the behavior of the future system in the next control period and determines control actions through optimization of the cost function according to the system state variables [21]. This means that the MPC algorithm is significantly affected by system uncertainties, including external disturbances, because system uncertainties cause prediction errors in the system control behavior and may degrade the control performance [22].

An extended state observer (ESO) is a very effective method to compensate for the severe effects of parameter uncertainties in the PMSM by estimating the state variables and disturbances, including the load torque [23]-[24]. Thus, various ESO based MPC methods have been studied [25]-[26]. In [27], to minimize the impact of parameter uncertainties, improved MPC algorithms were presented to increase the robustness and enhance the control performance under load parameter uncertainty. However, these methods focus on affecting only one parameter uncertainty in the control performance. In general, most system models are not specific to a particular parameter, so all parameter uncertainties and disturbances must be estimated using an observer to achieve high control performance. On the other hand, in [13], a simple disturbance observer was designed to estimate parameter uncertainties and used for a calculation of reference voltage. However, this method was designed to compensate only for electrical parameter uncertainties and did not consider all system uncertainties, owing to the complexity of the control structure. Therefore, a simple controller design is required to estimate all system parameter uncertainties and disturbances [28].

In this paper, an ESO based model predictive velocity control is proposed to achieve high control performance under disturbances and parameter uncertainties in a PMSM. We propose a single MPC that integrates the control of both velocity and current in a non-cascade structure. This innovative approach to velocity control applies a newly defined acceleration-based PMSM model to design a robust unified controller that effectively compensates for disturbances with partial system information. Utilizing the new model, a external disturbance and acceleration dynamics, including parameter uncertainties, can be lumped into the disturbance. By estimating the state variables and disturbance using the ESO, the MPC determines the optimal control input by predicting the behavior of the future system. The direct current controller is designed for the direct current to zero using feedback linearization and ESO-based MPC, operating within an independent reference frame. Thus, the combination of the new model and ESO based MPC improves the velocity tracking performance using the nominal input parameter. Also, because the proposed method is not designed based on the cascade structure from the viewpoint of velocity control, the optimization control for the velocity and currents can be obtained. Therefore, the proposed method is robust against external disturbances and parameter uncertainties owing to feedback linearization, state feedback, and ESO based MPC for the new PMSM model. The performance of the proposed method is validated via experiments.

The main contributions are summarized as follows:

- Unlike conventional PMSM model approaches that depend on precise system information, our method employs a acceleration dynamics to use only input parameter information and merge in the inner and outer loop, achieving high control performance under external disturbance and parameter uncertainties.
- The proposed control strategy enhances the robustness of MPC against external disturbance and parameter uncertainties by estimating a lumped disturbance, effectively compensating for system uncertainties.
- The newly developed PMSM model, incorporating acceleration dynamics, eliminates the need for additional control design while ensuring optimal velocity control.
- The direct current control based on ESO-based MPC improves the control performance while minimizing the requirement for precise system information, thereby significantly reducing system dependency.

II. PMSM MODEL AND PROBLEM FORMULATION

A. MATHEMATICAL MODEL OF PMSM

Consider the mathematical PMSM model represented in the $d-q$ frame as follows:

$$\begin{aligned}\dot{\omega} &= \frac{1}{J}\left[K_m i_q - B\omega - \tau_L\right] \\ \dot{i_q} &= \frac{1}{L}\left[v_q - Ri_q - P\omega L i_d - K_e\omega\right] \\ \dot{i_d} &= \frac{1}{L}\left[v_d - Ri_d + P\omega L i_q\right]\end{aligned} \tag{1}$$

where ω is the angular velocity (rad/s), B is the viscous friction coefficient (N·m·s/rad), J is the inertia of the motor (kg·m/rad), K_m is the torque constant (rad/s), R is the phase winding resistance (Ω), L is the phase winding inductance (H), P is the number of rotor teeth, τ_L is the load torque (NÂům), and i_q, i_d, and v_q, v_d are the direct and quadrature currents (A) and voltages (V). The load torque perturbation is denoted by τ_L. The derivative of the load torque τ_L with respect to time exists and is bounded, i.e., $\dot{\tau_L} = \delta_\tau$ is bounded, but unknown. Among the PMSM parameters, only the nominal value of is known. The PMSM model (1) is a third-order system with the phases d and q voltage inputs and velocity output.

B. MODEL REPRESENTATION AND PROBLEM FORMULATION

The acceleration α is defined as

$$\begin{aligned}\alpha &= \dot{\omega} \\ &= \frac{1}{J}\left(K_m i_q - B\omega - \tau_L\right). \end{aligned} \tag{2}$$

From (2), the new PMSM is obtained as

$$\begin{aligned}\dot{\omega} =& \alpha \\ \dot{\alpha} =& \frac{1}{JL}[K_m v_q - (JR + LB)\alpha - (BR + K_m K_e \\ & - K_m L P i_d)\omega - R\tau_L - L\dot{\tau}_L]. \end{aligned} \tag{3}$$

We define the input gain g_q as

$$g_q = \frac{K_m}{JL} = g_{qo} + \Delta g_q \tag{4}$$

where g_{qo} is the nominal value of g_q and Δg_q represents the uncertainties in g_q. From (1)-(4), the new model of PMSM is obtained as

$$\begin{aligned}\dot{x}_1 &= x_2 \\ \dot{x}_2 &= (g_{qo} + \Delta g_q)u - \frac{1}{JL}[(JR + LB)x_2 + (BR + K_m K_e \\ & - K_m L P i_d)x_1 + R\tau_L + L\dot{\tau}_L] \end{aligned} \tag{5}$$

where $x_1 = \omega$ and $x_2 = \alpha$. In (5), the disturbance $d_q = x_3$ is defined as

$$\begin{aligned}x_3 = \Delta g_q v_q - \frac{1}{JL}[(JR + LB)x_2 + (BR + K_m K_e \\ - K_m L P i_d)x_1 + R\tau_L + L\dot{\tau}_L]. \end{aligned} \tag{6}$$

Assumption 1: The derivative of the lumped disturbance x_3 is varying and bounded since x_3 include τ_L, i.e., $\dot{x}_3$, is bounded but unknown.

From Assumption 1, $\dot{x}_3 = \delta_q$ is bounded. All state variables in most systems are physically bounded, because the input is bounded in a practical system [28]. Therefore, it is reasonable that the lumped disturbance d_q composed of a linear combination of the state variable and parameter is bounded. Therefore, there exists an upper positive bound such that $sup|\delta_q(t)| = \delta_{q,max}$. The PMSM model (1) for velocity control without considering i_d is defined as

$$\begin{aligned}\dot{x}_1 &= x_2 \\ \dot{x}_2 &= g_{qo} v_q + x_3 \end{aligned} \tag{7}$$

where $x = [x_1, x_2, x_3]^T$ is the state vector. The aim is to make the velocity x_1 tracks the desired velocity x_{1d} using only the information of g_{qo}.

Remark 1: Generally, i_d is controlled to a given reference (typically zero) because it represents internal dynamics from the viewpoint of velocity control. Therefore, an additional controller design is required to ensure that i_d converges to zero.

III. ESO BASED MPC CONTROLLER

A. VELOCITY TRACKING CONTROL USING ESO BASED MPC

Using EulerâĂŹs law, the new normal form of the PMSM for velocity control in discrete-time is obtained as follows:

$$\begin{aligned}x_e(k+1) &= A_e x_e(k) + B_e v_q(k) \\ y_e(k) &= C_e x_e(k) \end{aligned} \tag{8}$$

where

$$A_e = \begin{bmatrix} 1 & T_s & 0 \\ 0 & 1 & T_s \\ 0 & 0 & 1 \end{bmatrix}, B_e = \begin{bmatrix} 0 \\ g_o T_s \\ 0 \end{bmatrix}, C_e = \begin{bmatrix} 1 & 0 & 0 \end{bmatrix}.$$

$x_e = [x_1 \;\; x_2 \;\; x_3]^T$ is the state variable vector, k is the time index, and T_s is the sampling time. An ESO is used to estimate the lumped disturbance for the MPC. The estimation state variable vector $\hat{x}_e$ is defined as

$$\hat{x}_e = \begin{bmatrix} \hat{x}_1 & \hat{x}_2 & \hat{x}_3 \end{bmatrix}^T. \tag{9}$$

Using (7) and (8), the ESO in the discrete-time model is designed as follows:

$$\begin{aligned}\hat{x}_e(k+1) =& A_e \hat{x}_e(k) + B_e v_q(k) + L(y_e(k) - \hat{y}_e(k)) \\ y_e(k) =& C_e \hat{x}_e(k) \end{aligned} \tag{10}$$

where

$$L = \begin{bmatrix} l_1 T_s & l_2 T_s & l_3 T_s \end{bmatrix}^T.$$

L is an observer gain. We assume that $d(k+1) = d(k) + \Delta d(k)$ where $\Delta d(k) \leq \delta_{max}$. Therefore, the estimation errors are defined as

$$\tilde{x}_e = x_e - \hat{x}_e = \begin{bmatrix} \tilde{x}_1 \\ \tilde{x}_2 \\ \tilde{x}_3 \end{bmatrix} = \begin{bmatrix} x_1 - \hat{x}_1 \\ x_2 - \hat{x}_2 \\ x_3 - \hat{x}_3 \end{bmatrix}. \tag{11}$$

From (8)-(11), the estimation error dynamics can be defined as

$$\tilde{x}_e(k+1) = A_o \tilde{x}_e(k) + D\delta \tag{12}$$

where

$$D = \begin{bmatrix} 0 \\ 0 \\ 1 \end{bmatrix}, \quad \delta = \frac{d(k+1) - d(k)}{T_s},$$

$A_o = A_e - LC_e$. If the observer gain L is set to be the eigenvalues of A_o in a unit circle, $\tilde{x}_e$ converges to the bounded ball. As an augmented model for the MPC, $x_q(k)$ is defined as the amount of change in the state variable and the output as follows:

$$x_q(k) = \begin{bmatrix} \Delta x_1(k) \\ \Delta x_2(k) \\ y_e(k) \end{bmatrix} \tag{13}$$

where $\Delta x_i(k) = x_i(k) - x_i(k-1)$, $i = [1 \;\; 2]$ and $y_e(k)$ is the velocity as output. Using (13), the augmented model is defined as

$$\begin{aligned} x_q(k+1) &= A_q x_q(k) + B_q \Delta v_q(k) + H_q \Delta \hat{x}_3(k) \\ y_q(k) &= C_q x_q(k) \end{aligned} \tag{14}$$

where

$$A_q = \begin{bmatrix} 1 & T_s & 0 \\ 0 & 1 & 0 \\ 1 & T_s & 1 \end{bmatrix}, B_q = \begin{bmatrix} 0 \\ g_{qo} T_s \\ 0 \end{bmatrix},$$
$$H_q = \begin{bmatrix} 0 \\ T_s \\ 0 \end{bmatrix}, C_q = \begin{bmatrix} 0 & 0 & 1 \end{bmatrix}.$$

The predicted output is obtained by using the calculated future state of the system in the augmented model (14). The predictive output is defined as

$$Y_q = F_q x_q(k) + \Phi_q \Delta v_q(k) + L_q \Delta \hat{x}_3(k) \tag{15}$$

where

$$F_q = \begin{bmatrix} C_q A_q & C_q A_q^2 & C_q A_q^3 & \cdots & C_q A_q^{N_p} \end{bmatrix}^T,$$
$$\Phi_q = \begin{bmatrix} C_q B_q & 0 & \cdots & 0 \\ C_q A_q B_q & C_q B_q & \cdots & 0 \\ C_q A_q^2 B_q & C_q A_q B_q & \cdots & 0 \\ \vdots & \vdots & \ddots & \vdots \\ C_q A_q^{N_q-1} B_q & C_q A_q^{N_q-2} B_q & \cdots & C_q A_q^{N_p-N_c} B_q \end{bmatrix},$$
$$L_q = \begin{bmatrix} C_q H_q & 0 & \cdots & 0 \\ C_q A_q H_q & C_q H_q & \cdots & 0 \\ C_q A_q^2 H_q & C_q A_q H_q & \cdots & 0 \\ \vdots & \vdots & \ddots & \vdots \\ C_q A_q^{N_p-1} H_q & C_q A_q^{N_p-2} H_q & \cdots & C_q A_q^{N_p-N_c} H_q \end{bmatrix}. \tag{16}$$

N_p is the prediction horizon and N_c is the control horizon. Using (15), the cost function that reflects the control objective is defined as

$$J_q = (R_s - Y_q)^T (R_s - Y_q) + \Delta v_q^T \bar{R}_q \Delta v_q,$$
$$\bar{R}_q = \begin{bmatrix} r_w & \cdots & 0 \\ \vdots & \ddots & \vdots \\ 0 & \cdots & r_w \end{bmatrix}, R_s^T = \begin{bmatrix} 1 & 1 & \cdots & 1 \end{bmatrix} r(k_i) \tag{17}$$

where $\bar{R}_q$ is the weight matrices and R_s is the reference of control. To find the optimal value of Δv_q that minimizes J_q, the first derivative of the cost function is zero. Thus, the optimal solution for the control signal is obtained as

$$\Delta v_q = (\Phi_q^T \Phi_q + \bar{R}_q)^{-1} \Phi_q^T (R_s - F_q x_q(k_i) - L_q \Delta \hat{x}_3(k)). \tag{18}$$

Finally, the velocity control input through the MPC is defined as

$$v_q(k+1) = v_q(k) + \Delta v_q \tag{19}$$

where $v_q(k)$ is the velocity control input for velocity tracking.

B. DIRECT CURRENT CONTROLLER USING ESO BASED MPC

A feedback linearization for v_d is designed to remove the coupled quadrature current as follows:

$$v_d = u_d - PL\omega i_q. \tag{20}$$

Similarly, in (7), i_d can be defined as

$$\dot{i}_d = g_{do} u_d + d_d \tag{21}$$

where g_{do} is the nominal value of g_d, $g_d = \frac{1}{L} = g_{do} + \Delta g_d$, and Δg_d denotes the uncertainties of g_d. d_d is the lumped disturbance for the i_d dynamics. The lumped disturbance is defined as the uncertainty of the input parameter and the system information. The lumped disturbance d_d is

$$d_d = \frac{R}{L} i_d + \Delta g_d. \tag{22}$$

The i_d dynamics model of PMSM in discrete-time is also defined as

$$i_d(k+1) = i_d(k) + T_s g_{do} u_d(k) + T_s d_d(k). \tag{23}$$

The ESO is used to estimate the lumped disturbance because the lumped disturbance is difficult to know exactly. The state variable vector is $x_d = [i_d, d_d]^T$, and the estimation state variable vector is $\hat{x}_d = [\hat{i}_d, \hat{d}_d]^T$. The ESO in the discrete-time model is designed as follows:

$$\begin{aligned} \hat{x}_d(k+1) &= A_c \hat{x}_d(k) + B_c u_d(k) + L_c(y_d(k) - \hat{y}_d(k)) \\ y_d(k) &= C_c \hat{x}_d(k) \end{aligned} \tag{24}$$

where

$$A_c = \begin{bmatrix} 1 & 0 \\ 0 & 1 \end{bmatrix}, \quad B_c = \begin{bmatrix} g_{do} T_s \\ 0 \end{bmatrix},$$
$$L_c = \begin{bmatrix} l_{d1} T_s & l_{d2} T_s \end{bmatrix}^T, \quad C_c = \begin{bmatrix} 1 & 0 \end{bmatrix}.$$

y_d is the direct current as output and L_c is an observer gain. The estimation errors are defined as

$$\tilde{x}_d = x_d - \hat{x}_d = \begin{bmatrix} \tilde{i}_d \\ \tilde{d}_d \end{bmatrix} = \begin{bmatrix} i_d - \hat{i}_d \\ d_d - \hat{d}_d \end{bmatrix}. \tag{25}$$

From (24) and (25), the estimation error dynamics can be defined as

$$\tilde{x}_d(k+1) = A_{do} \tilde{x}_d(k) + D_d \delta_d \tag{26}$$

where

$$D_d = \begin{bmatrix} 0 \\ 1 \end{bmatrix}, \quad \delta_d = \frac{d_d(k+1) - d_d(k)}{T_s}, \tag{27}$$

$A_{do} = A_c - L_c C_c$. If the observer gain, L_c is set to the eigenvalues of A_{do} in a unit circle, $\tilde{x}_d$ converges to the bounded ball. i_d is controlled to converge to zero by the MPC. In the augmented model, $x_d(k)$ is defined as the amount of change of i_d and the output.

$$x_d(k)^T = \begin{bmatrix} \Delta i_d(k)^T \\ i_d(k) \end{bmatrix} \tag{28}$$

where $\Delta i_d(k) = i_d(k) - i_d(k-1)$ and $i_d(k)$ is the output. Therefore, using (23), the augmented model for i_d is defined as

$$\begin{aligned} x_d(k+1) &= A_d x_d(k) + B_d u_d(k) + H_d \Delta \hat{d}_d(k) \\ y_d(k) &= C_d x_d(k) \end{aligned} \tag{29}$$

where

$$A_d = \begin{bmatrix} 1 & 0 \\ 1 & 1 \end{bmatrix}, \quad B_d = \begin{bmatrix} g_{do} T_s \\ g_{do} T_s \end{bmatrix}, \\ H_d = \begin{bmatrix} T_s \\ T_s \end{bmatrix}, \quad C_d = \begin{bmatrix} 0 & 1 \end{bmatrix}. \tag{30}$$

The prediction output is obtained using the calculated future state of the system in the augmented model (29). The predictive output is defined as

$$Y_d = F_d x_d(k) + \Phi_d \Delta u_d(k) + L_d \Delta \hat{d}_d(k) \tag{31}$$

where

$$F_d = \begin{bmatrix} C_d A_d & C_d A_d^2 & C_d A_d^3 & \cdots & C_d A_d^{N_p} \end{bmatrix}^T, \\ \Phi_d = \begin{bmatrix} C_d B_d & 0 & \cdots & 0 \\ C_d A_d B_d & C_d B_d & \cdots & 0 \\ C_d A_d^2 B_d & C_d A_d B_d & \cdots & 0 \\ \vdots & \vdots & \ddots & \vdots \\ C_d A_d^{N_p-1} B_d & C_d A_d^{N_p-2} B_d & \cdots & C_d A_d^{N_p-N_c} B_d \end{bmatrix}, \\ L_d = \begin{bmatrix} C_d H_d & 0 & \cdots & 0 \\ C_d A_d H_d & C_d H_d & \cdots & 0 \\ C_d A_d^2 H_d & C_d A_d H_d & \cdots & 0 \\ \vdots & \vdots & \ddots & \vdots \\ C_d A_d^{N_p-1} H_d & C_d A_d^{N_p-2} H_d & \cdots & C_d A_d^{N_p-N_c} H_d \end{bmatrix}. \tag{32}$$

Subsequently, using (31), the cost function that reflects the control objective is defined as

$$J_d = (R_d - Y_d)^T (R_d - Y_d) + \Delta u_d^T \bar{R}_d \Delta u_d, \\ \bar{R}_d = \begin{bmatrix} r_w & \cdots & 0 \\ \vdots & \ddots & \vdots \\ 0 & \cdots & r_w \end{bmatrix}, R_d^T = \begin{bmatrix} 1 & 1 & \cdots & 1 \end{bmatrix} r(k_i) \tag{33}$$

where $\bar{R}_d$ denotes the weight matrices and R_d is the reference of control. To find the optimal Δu_d that minimizes J_d, the first derivative of the cost function is zero. Thus, the optimal solution for the control signal i_d is obtained as

$$\Delta u_d = (\Phi_d^T \Phi_d + \bar{R}_d)^{-1} \Phi_d^T (R_d - F_d x_d(k_i) - L_d \Delta \hat{d}_d(k)). \tag{34}$$

Finally, the direct current control input for MPC is defined as

$$u_d(k+1) = u_d(k) + \Delta u_d. \tag{35}$$

Fig. 1 shows a block diagram of the proposed method. The proposed control algorithm consists of two main parts, velocity tracking control and direct current control. For the velocity tracking controller, the ESO (10) estimates x_e using the feedback of x_1. Then, the MPC (19) generates the control input v_q using $\hat{x}_e$ and x_1. The direct current controller is designed so that the direct current converges to zero. Feedback linearization (20) removes the nonlinear coupled terms, and the ESO(24) estimates d_d using the feedback of i_d. Then, the MPC (35) makes the optimal control input u_d using $\hat{d}_d$ and i_d. Thus, the proposed method is designed using two MPCs to achieve high control performance.

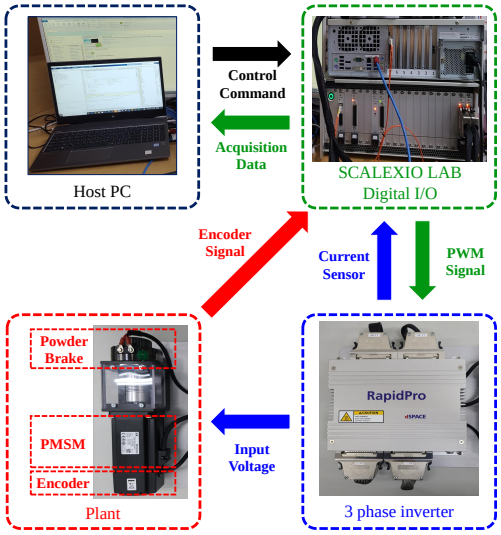

FIGURE 2. PMSM experimental testbed.

TABLE 1. Hardware specification.

RapidPro and SCALEXIO		
RapidPro	Max. voltage	60 V
	Max. current	60 A
	Max. switching freq.	50 kHz
	Number of legs (bridges)	4
SCALEXIO	System clock	3.8 GHz
	Number of cores	4
	Internal supply voltage	3.3, 5 V
	External power	12 V
	Number of DIO	36
	DIO input capture resolution	8 ns
	Number of ADCs	16
	ADC bit resolution	16
	ADC Max. conversion rate	4 MSPS
	ADC input range	Âś10 V

IV. EXPERIMENTAL RESULTS

Experiments were conducted to evaluate the control performance of the proposed method by using a PMSM driver set. The experimental setup consisted of a host computer with ControlDesk software, a three-phase inverter (Rapid-Pro), a PMSM (APM-SB03ADK-9, Kwapil and company), and the SCALEXIO real-time system manufactured by dSPACE

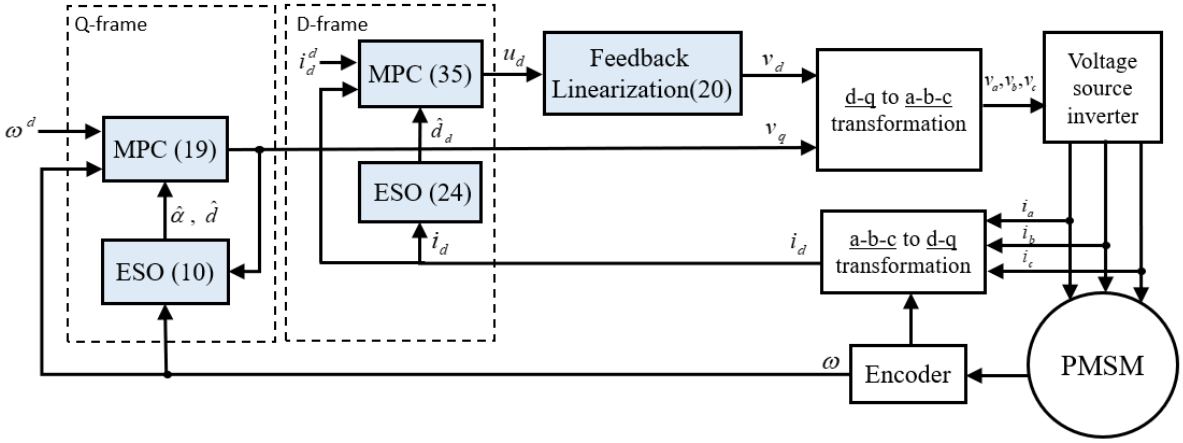

FIGURE 1. Block diagram of proposed method.

TABLE 2. Model parameter and control gain.

Parameter	Value	Gain	Value
J	4.675×10^{-4} [kg·m^2]	N_p	20
B	9×10^{-4} [N·m·s/rad]	N_c	2
R	0.2 [Ω]	l_{d1}	1280
L	0.4 [mH]	l_{d2}	4.08×10^5
K_m	0.102 [N·m/A]		
K_e	0.102 [N·m/A]		
p	4		

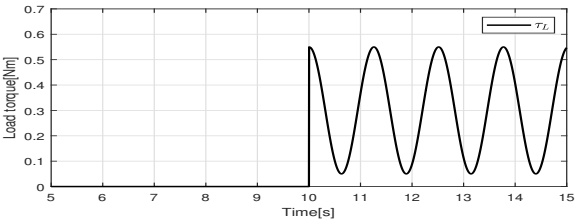

FIGURE 3. Load torque injected by the powder brake.

GmbH. A host computer was used to implement the control program generated through MATLAB/Simulink in C language, compile the program, and upload the executable output code to the SCALEXIO real-time system. The three-phase inverter(Rapid-Pro) consisted of three half bridge power stage modules. The PMSM was directly connected to an incremental encoder (2500 pulses/revolution). The switching frequency was set at 20 kHZ. Fig. 2 shows the hardware configuration of the PMSM driver set. The detailed hardware specifications are listed in Table 1. The parameters of the PMSM listed in Table 2 were used. The maximum desired angular velocity was 20π rad/s. The load torque, which is an external disturbance, was injected using a powder brake. The viscosity of the powder positioned between the rotor and stator was generated by the current applied to the powder brake. Therefore, the load torque injected by the powder brake can be expressed as

$$\tau_L = \begin{cases} 0 & (5 \le t < 10) \\ 0.25\sin\left(\frac{5\pi t}{2}\right) + 0.3 & (10 \le t \le 15) \end{cases} \tag{36}$$

The load torque τ_L was injected, as shown in Fig.3.

The following two cases were conducted to evaluate the performance of the proposed method.

1) Case 1: Velocity tracking control ESO based MPC using conventional PMSM model.
2) Case 2: Proposed method.

In Case 1, the nominal PMSM model was used through MPC based on an ESO. The feedback linearization for the $d-q$ input voltages was designed to remove coupled nonlinear terms as follows:

$$\begin{aligned} v_d &= u_d - pL\omega i_q \\ v_q &= u_q + pL\omega i_d. \end{aligned} \tag{37}$$

The disturbance in velocity dynamics was defined as

$$d = \tau_L. \tag{38}$$

The ESO was defined as

$$\begin{aligned} \hat{\omega}(k+1) &= \hat{\omega}(k) - \frac{T_s}{J}\left[-B\hat{\omega}(k) + K_m i_q(k) - \hat{d}(k)\right] \\ &\quad + T_s l_{q1}(\omega(k) - \hat{\omega}(k)) \\ \hat{i}_q(k+1) &= \hat{i}_q(k) + \frac{T_s}{L}\left[-K_e\hat{\omega}(k) - R\hat{i}_q(k) + v_q(k)\right] \\ &\quad + T_s l_{q2}(\omega(k) - \hat{\omega}(k)). \end{aligned} \tag{39}$$

The control input for velocity control was defined as

$$u_q(k+1) = u_q(k) + \Delta u_q \tag{40}$$

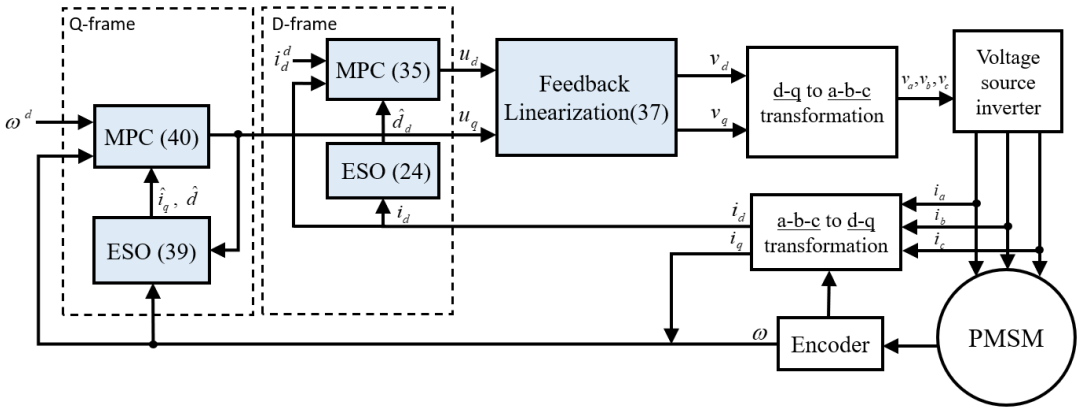

FIGURE 4. Block diagram of Case 1.

where Δu_q was obtained from the MPC cost function. This controller was designed to compensate for only mechanical disturbance, τ_L, using the ESO. The direct current control was designed to be the same as that in the proposed method. The observer gains were set as l_{q1} = 1.518 $\times 10^3$, l_{q2} = -301.2. The observer gains for i_d and the MPC gains listed in Table 1 were used. A block diagram of the Case 1 algorithm is shown in Fig. 4.

In Case 2, the proposed control algorithm was used. The observer gains were set as l_1 = 2022, l_2 = 1.3$\times 10^6$, and l_3 = 3.05$\times 10^8$. Same as in Case 1, the observer gains for i_d and the MPC gains listed in Table 1 were used.

Experiments were conducted to validate the velocity-tracking performance of all cases. The experiments were conducted under the following two scenarios:

1) Scenario 1: Velocity control was conducted without parameter uncertainties.
2) Scenario 2: Velocity control was conducted with 30% parameter uncertainties.

A. SCENARIO 1

The model parameters used in the experiment are the above mentioned values, in which τ_L represents the load torque. Fig. 5 shows the velocity tracking error, $e_\omega = \omega - \omega_d$. The peaks of velocity tracking in both Cases appeared at t = 10 due to the injected load torque, but both peaks rapidly decreased. On the other hands, Although the tracking error peaks in Case 2 were slightly larger than those in Case 1, the velocity tracking in both Cases had similar control performance. Fig. 6 shows the estimated lumped disturbance in the velocity tracking controller. Compared to Case 1, the estimated lumped disturbance in Case 2 had large values because all parameter uncertainties except for the input parameter were designed to be estimated. After 10 s, when the load torque was injected, the oscillation of the estimated lumped disturbance in both Cases was accompanied by the load torque. Although the estimated disturbance in Case 1 was only load torque, the

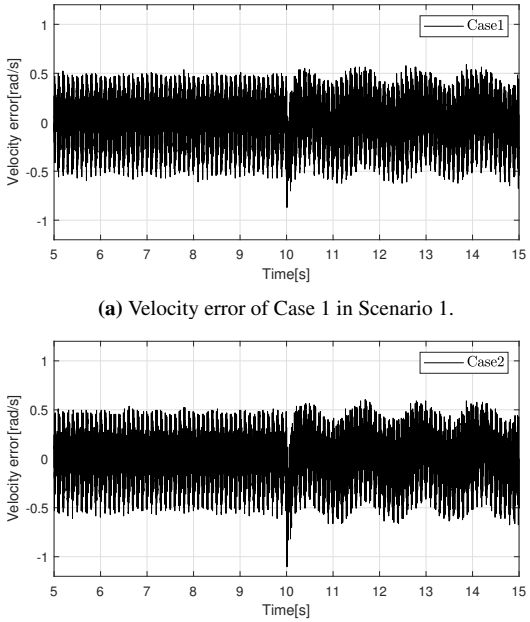

(a) Velocity error of Case 1 in Scenario 1.

(b) Velocity error of Case 2 in Scenario 1.

FIGURE 5. Velocity errors in Cases 1-2 in Scenario 1.

estimated lumped disturbance in Case 1 had higher values than the injected load torque shown in Fig. 3 because of several unavoidable reasons, such as non-ideal sinusoidal flux disturbance and ripples of pulse width modulation. Fig. 7 shows the direct current and estimated lumped disturbance in the direct current controller. The direct current controllers in both Cases had similar and satisfactory control performance because the same controller was applied. The input voltages are shown in Fig. 8. Direct voltages in both Cases also had similar values because estimated lumped disturbances in the direct current controller in both Cases had similar values.

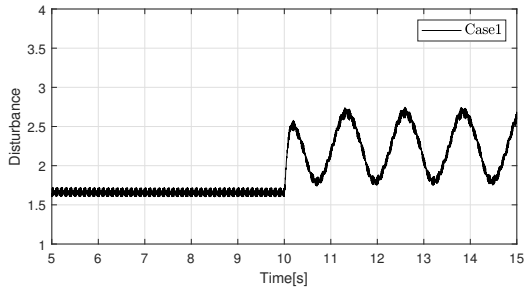

(a) Estimated lumped disturbances in Case 1.

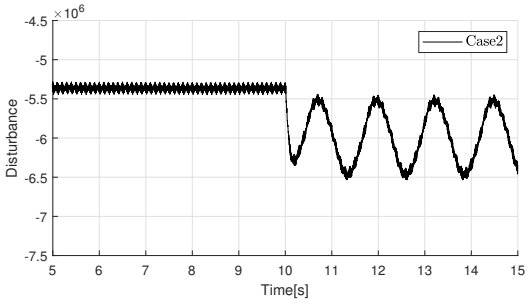

(b) Estimated lumped disturbances in Case 2.

FIGURE 6. Estimated lumped disturbances in velocity dynamics of Cases 1-2 in Scenario 1.

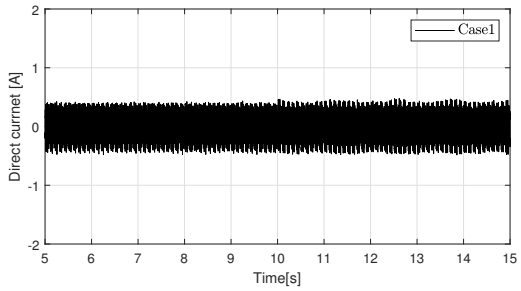

(a) Direct current of Case 1 in Scenario 1.

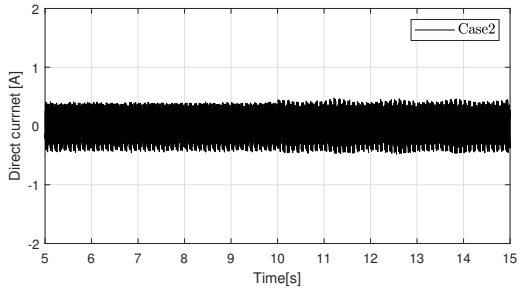

(b) Direct current of Case 2 in Scenario 1.

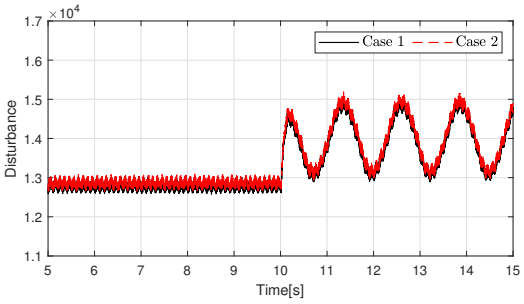

(c) Estimated lumped disturbance of both cases.

FIGURE 7. Direct current and lumped disturbance in direct current dynamics of Cases 1-2 in Scenario 1.

B. SCENARIO 2

In Scenario 2, to validate the robustness of the performance of the proposed method, the experiment was performed with 30% parameter uncertainties. The other parameters were the same as those in Scenario 1. Velocity tracking errors are shown in Fig. 9. The magnitude of the ripples of the velocity tracking error in Case 1 increased than in Case 2. The tracking error in Case 1 increased by 10% compared to that in Case 2 at 5-10 seconds and increased by 25% at 10-15 seconds after injecting the load torque. Meanwhile, the ripple of the velocity tracking error in Case 2 exhibited no obvious change compared to Scenario 1. It can be seen that the control algorithm in Case 2 was robust to system uncertainties, whereas the controller in Case 1 was susceptible to parameter uncertainties. In other words, the existence of parameter uncertainties in Case 1 led to a velocity tracking error, which aggravates the control performance of the entire control system. Fig. 10 shows the estimated lumped disturbance for the velocity tracking controller. The estimated lumped disturbances in both Cases had more oscillations than in Scenario 1 due to parameter uncertainties. Fig. 11 shows the direct current and estimated lumped disturbances in the direct current controller. The direct current in Case 1 was smaller than that in Scenario 1 because the input parameter was set to increase. Meanwhile, in Case 2, the direct current was similar to that in Scenario 1 because the lumped disturbance values in the direct current controller were reduced compared to those in Scenario 1. Although the direct current controller in Case 1 had better control performance than that in Case 2, the velocity tracking control in Case 2 was significantly more robust than that in Case 1 because the direct current was an internal dynamic of the PMSM. The voltages are shown in Fig. 12. The voltage values in both Cases were similar to those in Scenario 1, even under parameter uncertainties. Therefore, the quadrature voltage in Case 2 was slightly reduced because the parameter uncertainties were set by increasing the input parameter.

V. CONCLUSION

In this paper, we proposed an ESO based model predictive velocity control to achieve high control performance under disturbance and parameter uncertainties for a new PMSM. The proposed method was designed to estimate the lumped disturbance based on the new PMSM model that uses acceleration dynamics instead of quadrature current dynamics. Thus, the proposed velocity tracking controller compensated for the uncertainties of the entire PMSM because it was not designed based on a cascade structure. The experimental results showed that the proposed control algorithm is robust against parameter uncertainties. Although ripples were caused by several unavoidable factors, including low encoder resolution, pulse width modulation ripples, and non-ideal sinusoidal

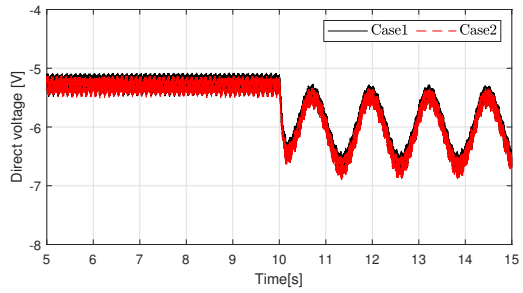

(a) Direct voltage in Scenario 1.

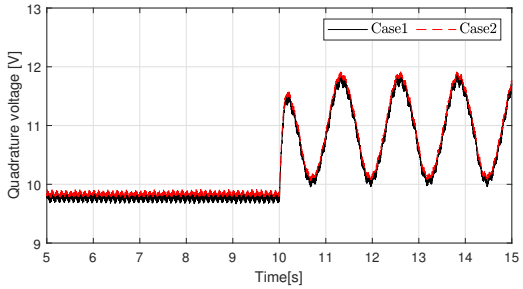

(b) Quadrature voltage in Scenario 1.

FIGURE 8. Direct and quadrature voltages of Cases 1-2 in Scenario 1.

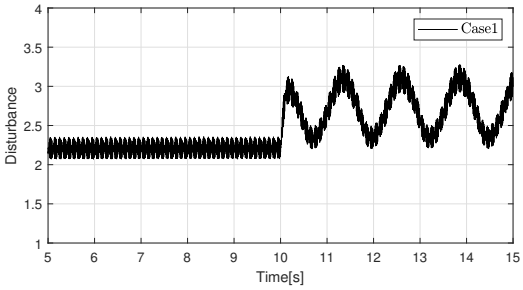

(a) Estimated lumped disturbances in Case 1.

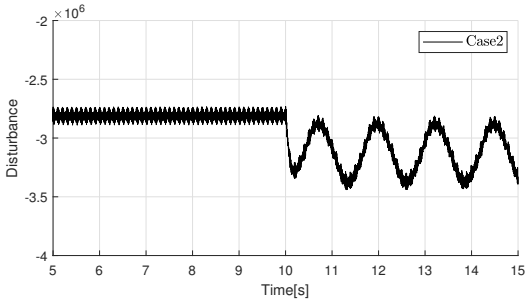

(b) Estimated lumped disturbances in Case 2.

FIGURE 10. Estimated lumped disturbances in velocity dynamics of Cases 1-2 in Scenario 2.

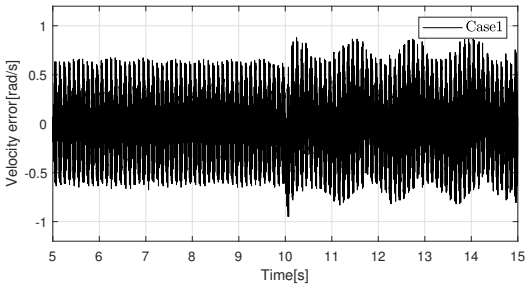

(a) Velocity error of Case 1 in Scenario 2.

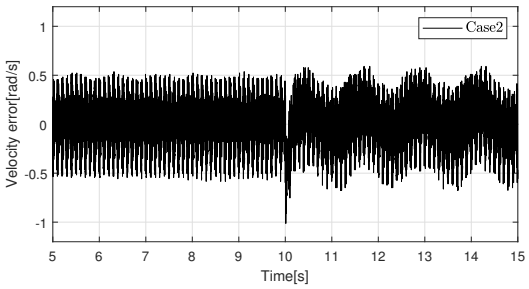

(b) Velocity error of Case 2 in Scenario 2.

FIGURE 9. Velocity errors in Cases 1-2 in Scenario 2.

flux disturbances, the velocity tracking errors of the proposed method were small in the steady state responses compared to the conventional PMSM model. The combination of the new model and ESO based MPC improved the velocity tracking performance.

REFERENCES

[1] X. Liu, H. Yu, J. Yu, and L. Zhao, "Combined speed and current terminal sliding mode control with nonlinear disturbance observer for PMSM drive," *IEEE Access*, vol. 6, pp. 29594–29601, 2018.

[2] M. H. Vafaie, "Performance improvement of permanent-magnet synchronous motor through a new online predictive controller," *IEEE Trans. Energy Convers.*, vol. 34, no. 4, pp. 2258–2266, Dec. 2019.

[3] J. Yim, S. You, Y. Lee, and W. Kim, "Chattering attenuation disturbance observer for sliding mode control: Application to permanent magnet synchronous motors," *IEEE Trans. Ind. Electron.*, vol. 70, no. 5, pp. 5161–5170, May 2023.

[4] S. Li and Z. Liu, "Adaptive speed control for permanent-magnet synchronous motor system with variations of load inertia," *IEEE Trans. Ind. Electron.*, vol. 56, no. 8, pp. 3050–3059, Aug. 2009.

[5] X. Zhang, L. Sun, K. Zhao, and L. Sun, "Nonlinear speed control for PMSM system using sliding-mode control and disturbance compensation techniques," *IEEE Trans. Power Electron.*, vol. 28, no. 3, pp. 1358–1365, Mar. 2013.

[6] J. Gil, S. You, Y. Lee, and W. Kim, "Super twisting-based nonlinear gain sliding mode controller for position control of permanent-magnet synchronous motors," *IEEE Access*, vol. 9, pp. 142060–142070, 2021.

[7] S. You, J. Gil, and W. Kim, "Adaptive neural network control using nonlinear information gain for permanent magnet synchronous motors," *IEEE Trans. Cybern.*, vol. 53, no. 3, pp. 1394–1404, Mar. 2023.

[8] M. Morawiec, "The adaptive backstepping control of permanent magnet synchronous motor supplied by current source inverter," *IEEE Trans. Ind. Informat.*, vol. 9, no. 2, pp. 1047–1055, May. 2013.

[9] A. V. Sant and K. R. Rajagopal, "PM synchronous motor speed control using hybrid fuzzy-PI with novel switching functions," *IEEE Trans. Magn.*, vol 45, no. 10, pp. 4672–4675, Oct. 2009.

[10] W. Kim, D. Shin, and C. Chung, "Microstepping using a disturbance observer and a variable structure controller for permanent magnet stepper

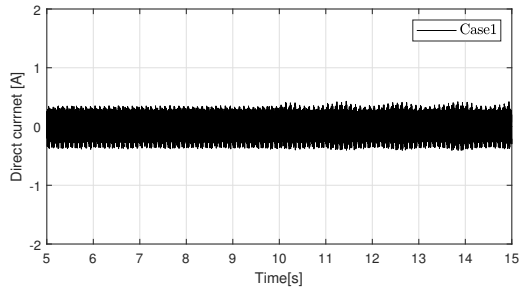

(a) Direct current of Case 1 in Scenario 2.

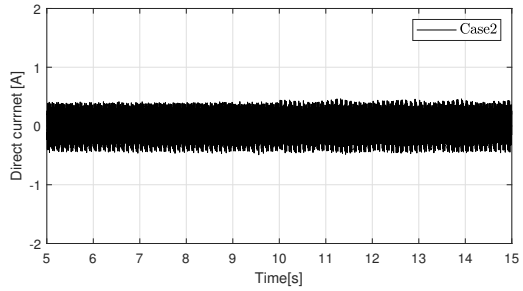

(b) Direct current of Case 2 in Scenario 2.

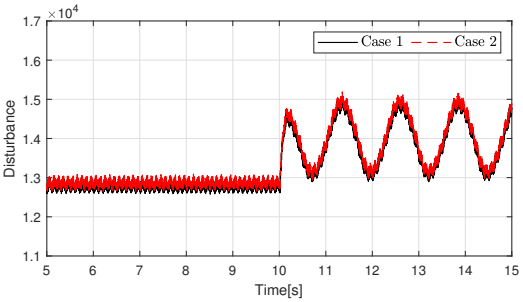

(c) Estimated lumped disturbance of both cases.

FIGURE 11. Direct current and lumped disturbance in direct current dynamics of Cases 1-2 in Scenario 2.

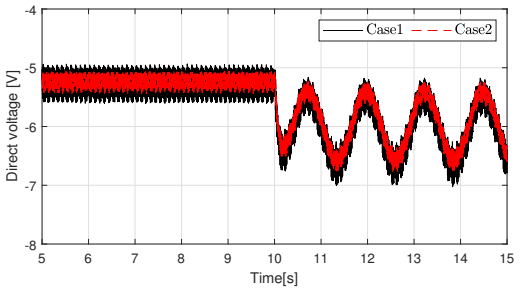

(a) Direct voltage in Scenario 2.

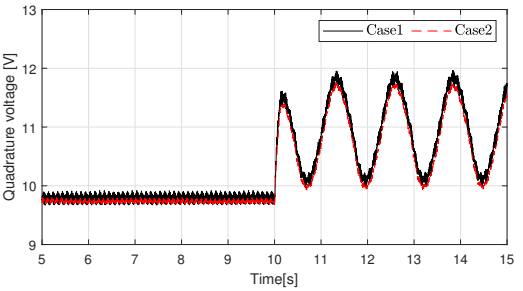

(b) Quadrature voltage in Scenario 2.

FIGURE 12. Voltages of Cases 1-2 in Scenario 2.

motors," *IEEE Trans. Ind. Electron.*, vol. 60, no. 7, pp. 2689–2699, Jul. 2013.

[11] K. Kim and M. Youn, "A nonlinear speed control for a PM synchronous motor using a simple disturbance estimation technique," *IEEE Trans. Ind. Electron.*, vol. 49, no. 3, pp. 524–535, Jun. 2002.

[12] Y. Luo and C. Liu, "A simplified model predictive control for a dual three-phase PMSM with reduced harmonic currents," *IEEE Trans. Ind. Electron.*, vol. 65, no. 11, pp. 9079–9089, Nov. 2018.

[13] X. Zhang, L. Zhang, and Y. Zhang, "Model predictive current control for PMSM drives with parameter robustness improvement," *IEEE Trans. Power Electron.*, vol. 34, no. 2, pp. 1645–1657, Feb. 2012.

[14] H. Wang, B. Liu, X. Ping, and Q. An, "Path tracking control for autonomous vehicles based on an improved MPC," *IEEE Access*, vol. 7, pp. 161064–161073, 2019.

[15] S. Kouro, M. A. Perez, J. Rodriguez, A. M. Llor, and H. A. Young, "Model predictive control: MPC's role in the evolution of power electronics," *IEEE Ind. Electron. Mag.*, vol. 9, no. 4, pp. 8–21, Dec. 2015.

[16] A. Brosch, O. Wallscheid, and J. BÃűcker, "Model predictive control of permanent magnet synchronous motors in the overmodulation region including six-step operation," *IEEE Open J. Ind. Appl.*, vol. 2, pp. 47–63, 2021.

[17] S. Vazquez, E. Zafra, R. P. Aguilera, T. Geyer, J. I. Leon, and L. G. Franquelo, "Prediction model with harmonic load current components for FCS-MPC of an uninterruptible power supply," *IEEE Trans. Ind. Electron.*, vol. 37, no. 1, pp. 322–331, Jan. 2022.

[18] L. Wang, T. Zhao, and J. He, "Investigation of variable switching frequency in finite control set model predictive control on grid-connected inverters," *IEEE Open J. Ind. Appl.*, vol. 2, pp. 178–193, 2021.

[19] J. B. Rawlings, "Tutorial overview of model predictive control," *IEEE Control Syst. Mag.*, vol. 20, no. 3, pp. 38–52, Jun. 2000.

[20] M. Schwenzer, M. Ay, T. Bergs, and D. Abel, "Review on model predictive control: An engineering perspective," *Int. J. Adv. Manuf. Technol.*, vol. 117, no.5, pp.1327–1349, Aug. 2021.

[21] H. A. Young, M. A. Perez, and J. Rodriguez, "Analysis of finite-controlset model predictive current control with model parameter mismatch in a three-phase inverter," *IEEE Trans. Ind. Electron.*, vol. 63, no. 5, pp. 3100–3107, May 2016.

[22] X. Zhang and Z. Wu, "Two-stage model predictive current control for PMSM drives with parameter robustness improvement," *IEEE Trans. Energy Convers.*, vol. 39, no. 2, pp. 1352–1360, Jun. 2024.

[23] J. Li, L. Zhang, L. Luo, and S. Li, "Extended state observer based current-constrained controller for a PMSM system in presence of disturbances: Design, analysis and experiments," *Control Eng. Pract.*, vol. 132, 2023, Art. no. 105412.

[24] S. Li, H. Liu, and S. Ding, "A speed control for a PMSM using finite-time feedback control and disturbance compensation," *Trans. Inst. Meas. Control*, vol. 32, no. 2, pp. 170–187, Apr. 2010.

[25] M. Yang, X. Lang, J. Long, and D. Xu, "Flux immunity robust predictive current control with incremental model and extended state observer for PMSM drive," *IEEE Trans. Power Electron.*, vol. 32, no. 12, pp. 9267–9279, Dec. 2017.

[26] C. Jia, X. Wang, Y. Liang, and K. Zhou, "Robust current controller for IPMSM drives based on explicit model predictive control with online disturbance observer," *IEEE Access*, vol. 7, pp. 45898–45910, 2019.

[27] G. H. Bode, P. C. Loh, M. J. Newman, and D. G. Holmes, "An improved robust predictive current regulation algorithm," *IEEE Trans. Ind. Appl.*, vol. 41, no. 6, pp. 1720–1733, Dec. 2005.

[28] S. You, J. Gil, and W. Kim, "Extended state observer based robust position tracking control for DC motor with external disturbance and system uncertainties." *J. Elect. Eng. Technol.*, vol. 14, no. 4, pp. 1637–1646, 2019.

EUNJI LEE received the B.S degree from the School of Energy Systems Engineering, ChungAng University, Seoul, South Korea, in 2023, where she is currently pursuing the M.S. degree in energy systems engineering. Her research interests include nonlinear control, motor control, observer control, vehicle control, and their industrial applications.

YONGHAO GUI received a B.S. degree in automation from Northeastern University, Shenyang, China, in 2009, and the M.S. and Ph.D. degrees in electrical engineering from Hanyang University, Seoul, South Korea, in 2012 and 2017, respectively. He is with Oak Ridge National Laboratory (ORNL), USA. Dr. Gui has served as an Associate Editor for the IEEE Transactions on Industrial Electronics, IEEE Transactions on Sustainable Energy, and IEEE Transactions on Energy Conversion.

SESUN YOU received the B.S. and Ph.D. degrees from the School of Energy Systems Engineering, ChungAng University, Seoul, South Korea, in 2020 and 2024, respectively. He is currently an Assistant Professor with the Department of Electrical Engineering, Keimyung University, Daegu, South Korea. His research interests include nonlinear control, adaptive control, neural control, intelligent control for nonlinear systems, and their industrial applications.

JUN MOON received the B.S. degree in electrical and computer engineering and the M.S. degree in electrical engineering from Hanyang University, Seoul, South Korea, in 2006 and 2008, respectively, and the Ph.D. degree in electrical and computer engineering from the University of Illinois at UrbanaâĂŞChampaign, Champaign, IL, USA, in 2015. He is currently an Associate Professor with the Department of Electrical Engineering, Hanyang University. From February 2008 to June 2011, he was a Researcher with the Agency for Defense Development, Daejeon, South Korea. From February 2016 to February 2019, he was an Assistant Professor with the School of Electrical and Computer Engineering, Ulsan National Institute of Science and Technology, Ulsan, South Korea. From March 2019 to August 2020, he was Assistant and Associate Professors with the School of Electrical and Computer Engineering, University of Seoul, Seoul. His research interests include stochastic games, stochastic control and estimation, mean field games, distributed optimal control, networked control systems, and control of unmanned vehicles. Dr. Moon was the recipient of the Fulbright Graduate Study Award in 2011.

WONHEE KIM received the B.S. and M.S. degrees in electrical and computer engineering and the Ph.D. degree in electrical engineering from Hanyang University, Seoul, South Korea, in 2003, 2005 and 2012, respectively. From 2005 to 2007, he was with Samsung Electronics Company, Suwon, South Korea. In 2012, he was with the Power and Industrial Systems Research and Development Center, Hyosung Corporation, Seoul. In 2013, he was a Postdoctoral Researcher with the Institute of Nano Science and Technology, Hanyang University, and Visiting Scholar with the Department of Mechanical Engineering, University of California, Berkeley, CA, USA. From 2014 to 2016, he was with the Department of Electrical Engineering, Dong-A University, Busan, South Korea. He is currently a Professor with the School of Energy Systems Engineering, ChungAng University, Seoul. His research interests include nonlinear control and nonlinear observers, and their industrial applications. He was an Associate Editor for IEEE/ASME TRANSACTIONS ON MECHATRONICS, IEEE ACCESS, and Journal of Electrical Engineering & Technology.